JVST B
Journal of Vacuum Science & Technology B

ARTICLE

avs.scitation.org/journal/jvb

# Inks of dielectric h-BN and semiconducting $WS_2$ for capacitive structures with graphene

Cite as: J. Vac. Sci. Technol. B 38, 052201 (2020); doi: 10.1116/6.0000092
Submitted: 7 February 2020 · Accepted: 8 July 2020 ·
Published Online: 30 July 2020



Jay A. Desai,[1,2,3,4] Sangram Mazumder,[2,3] Ridwan Fayaz Hossain,[3] and Anupama B. Kaul[2,3,a)]

## AFFILIATIONS

[1]Department of Metallurgical, Materials and Biomedical Engineering, University of Texas at El Paso, El Paso, Texas 79968
[2]Department of Materials Science and Engineering, University of North Texas, Denton, Texas 76203
[3]Department of Electrical Engineering, and PACCAR Technology Institute, University of North Texas, Denton, Texas 76203
[4]Department of Metallurgical and Materials Engineering, VNIT, Nagpur, Maharashtra 440010, India

[a)]**Electronic mail:** anupama.kaul@unt.edu

## ABSTRACT

We present dispersions of $WS_2$ and h-BN using cyclohexanone and terpineol as the solvent to subsequently print prototype capacitive nanodevices. An all-inkjet-printing approach was used to print graphene-h-BN-graphene capacitors along with graphene-$WS_2$-graphene structures. As the number of passes for inkjet printing the h-BN layer within graphene electrodes was increased, the leakage currents successively decreased. The capacitance-frequency (*C-f*) measurement data for the printed capacitor (with 40 passes of h-BN) within graphene electrodes showed that at ~1 kHz, the maximum capacitance was ~62 pF, and with increasing frequency, the capacitance value decreases. The inkjet printed graphene-$WS_2$-graphene heterostructure devices were also constructed using horn tip sonication, where the *C-f* measurements revealed that *C* as high as ~324.88 pF was attainable, which was largely frequency independent up to ~20 kHz. This is in contrast with the h-BN layer integrated with graphene electrodes, where the measured *C* was more than ~5 times lower over the range of frequencies tested and also exhibited a strong decay as frequency increased from 1 kHz.



## I. INTRODUCTION

Since the first emergence of graphene, the two-dimensional (2D) allotrope of carbon, in 2004,[1,2] various other layered materials have been the center of attention, specifically transition metal dichalcogenides (TMDCs). These materials have successfully drawn great interest among researchers all over the world owing to their state-of-the-art electronic,[3] optical,[4] mechanical,[5] and chemical properties.[6] They are representative of a class of materials having the formula $MX_2$, where M is a transition metal element (e.g., Mo, W, Ti, V, or Nb) and X is a chalcogen (S, Se, or Te). Schematically, the TMDCs have a layered structure in the form of X-M-X, where one plane of the metal atoms is sandwiched by two planes of chalcogen atoms.[5] In several of these semiconducting TMDCs, such as $MoS_2$ and $WS_2$, an indirect-to-direct bandgap transition is noticed when the bulk layered material is exfoliated down to monolayers.[7,8] These TMDCs also display sizable bandgaps ranging within 1 to beyond 2 eV, which makes them very promising for many electronic and optoelectronic devices, potentially as alternatives to Si-based (bandgap ~1.14 eV) or GaAs-based (bandgap ~1.43 eV) devices.[9]

While a significant amount of work has already been conducted on $MoS_2$ exfoliation to better elucidate its optical and electronic properties,[10–14] the body of work on similar exfoliation studies on semiconducting $WS_2$ as well as dielectric h-BN, also a layered material, has been relatively sparse. For $WS_2$ in its bulk form, it exhibits an indirect bandgap of ~1.4 eV and undergoes a transition to a direct bandgap semiconductor with a bandgap of ~2.1 eV in the monolayer limit,[15] which makes it attractive for high-performance electronic and optoelectronic devices.[16–26]

Many of the 2D layered material based devices, including h-BN and $WS_2$, can be fabricated using bottom-up approaches such as physical vapor deposition[27] or chemical vapor deposition,[28] where the atomic species stack up to form the 2D nanosheets. However, these layered materials can also be manufactured using top-down approaches such as mechanical[29] or chemical exfoliation,[30] where the 2D atomic layer membranes emerge from the bulk crystal. The liquid-phase or chemical exfoliation of these and related materials have been seen to offer a range of advantages over other methods, which includes low processing cost, attractive scalability toward large

formats, their material conserving nature, and low-temperature processing even approaching room temperature.[31–33]

In this work, we have used additive manufacturing techniques to form capacitive structures with 2D atomic layers of h-BN where we have relied exclusively on inkjet printing. Kelly *et al.*[34] developed an approach to print pinhole-free, vertically stacked heterostructures using a hybrid approach of inkjet printing and spray-coating for graphene/BN/graphene capacitive structures that exhibited an aerial capacitance ranging from 0.24 to 1.1 nF/cm$^2$ with an average series resistance of 120 kW. Park *et al.*[35] fabricated metal-insulator-semiconductor capacitors with h-BN dielectric films grown using a high temperature plasma-enhanced atomic layer deposition process, where a capacitance density of up to ~0.13 $\mu$F/cm$^2$ and a current density of up to ~$10^{-3}$ A/cm$^2$ were reported. In our work, the horn tip (HT) sonication exfoliation route was used to exfoliate dielectric h-BN and semiconducting $WS_2$ along with conducting graphene inks. Inkjet printing was then used for the formation of capacitive structures comprised of h-BN and $WS_2$ nanosheets integrated with graphene electrodes. Raman and photoluminescence (PL) spectroscopy and optical absorption spectroscopy were used for the material analysis, while current-voltage, capacitance-voltage (*C-V*), and capacitance-frequency (*C-f*) measurements were used to characterize the capacitive structures comprised of inkjet printed h-BN and $WS_2$ layers.

## II. RESULTS AND DISCUSSION

### A. Dielectric h-BN and conducting graphene ink for capacitors

Cyclohexanone (70%) (Sigma Aldrich # 398241)/terpineol (30%) (Sigma Aldrich # 86480) solution (C/T) mixtures were prepared in 20 ml glass vials. Ethyl cellulose (EC), (2.5 wt. %) (Sigma Aldrich # 200646) was successively added to the solution and the system was bath sonicated for 2 h to ensure the complete dissolution of EC in the C/T solution mixture. This particular combination of C/T/EC has a viscosity of ~12 cP, ideal for inkjet printing, as it has been reported in our previous work.[30] For h-BN, the mixture was bath sonicated for 2 h to promote the complete and uniform mixing of EC in the C/T solution. The graphite (Sigma Aldrich # 496553) and h-BN (Sigma Aldrich # 255475) powders in a concentration of 30 mg/ml or 0.6 g were then taken in two separate 50 ml beakers, and 20 ml of the C/T/EC solution was added to both of the mixtures. The exfoliation technique used here is HT sonication, which exposes the layered material to ultrasonic waves in an appropriate solvent by inducing vibrations through a horn tip. Ultrasonic waves cause cavitation bubbles that eventually collapse into high energy jets, breaking up the layered crystallites to give rise to exfoliated nanosheets. HT sonication at 20% and 40% power amplitude is denoted as HT (low) and HT (high), respectively. HT (high) and magnetic stirring at 500 rpm for 3 h were then employed for the graphene and h-BN ink preparation. For the graphene ink, 15 passes were printed, whereas the h-BN was printed at passes varying from ~6, 12, 20, 30, and up to 40.

Figure 1(a) demonstrates the optical image of a 2 × 2 mm$^2$ inkjet printed h-BN structure on an $SiO_2$/Si substrate. Figure 1(b) shows the inkjet printed graphene-h-BN-graphene capacitor, where the h-BN layer is sandwiched in between the graphene layers. The optical absorption characteristics for the printed h-BN structure are shown in Fig. 2(a), which reveals that it is active in the UV regime, while graphene's optical activity is largely undetected into the visible regime from the data shown. Raman spectroscopy was used to characterize the material using a Horiba LabRAM HR Evolution Microscope. In Raman spectroscopy, the interaction of an incoming laser with the molecular vibrations of the material of interest causes a change in the energy of the outgoing reflected photons. This change in energy relays information about the unique vibrational modes and serves as a fingerprint for the material of interest.[36–41] The Raman spectra for printed graphene patterns at room temperature is shown in Fig. 2(b) exhibiting peaks at ~1350, ~1577, and ~2700 cm$^{-1}$ attributed to the D-band, G-band, and G'-band, respectively. The room temperature Raman spectra for the annealed and optimized h-BN layer is shown in Fig. 2(c), which

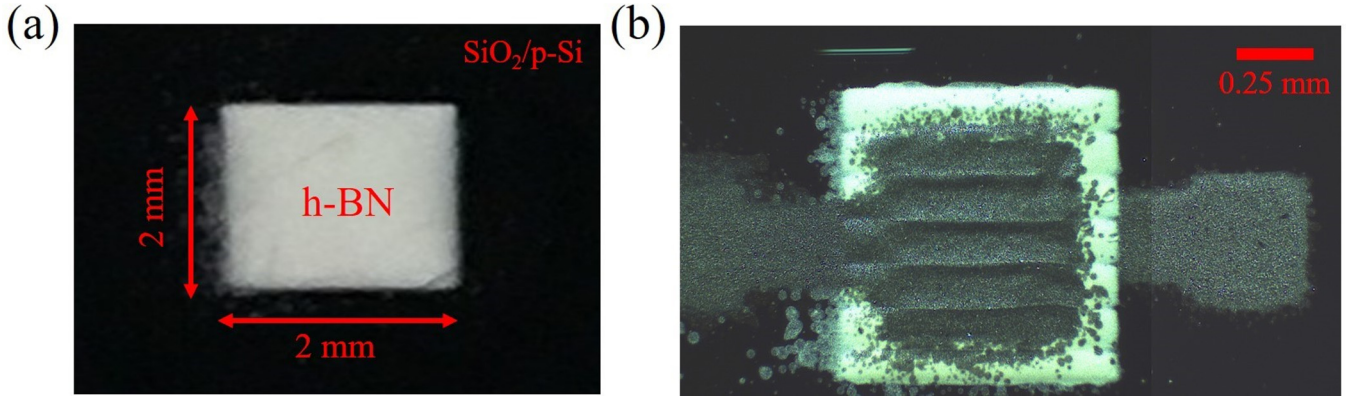


**FIG. 1.** (a) Optical image of a 2 × 2 mm$^2$ inkjet printed h-BN structure on an $SiO_2$/Si substrate. (b) Inkjet printed graphene-h-BN-graphene capacitor, where the h-BN layer is sandwiched in between the graphene layers.

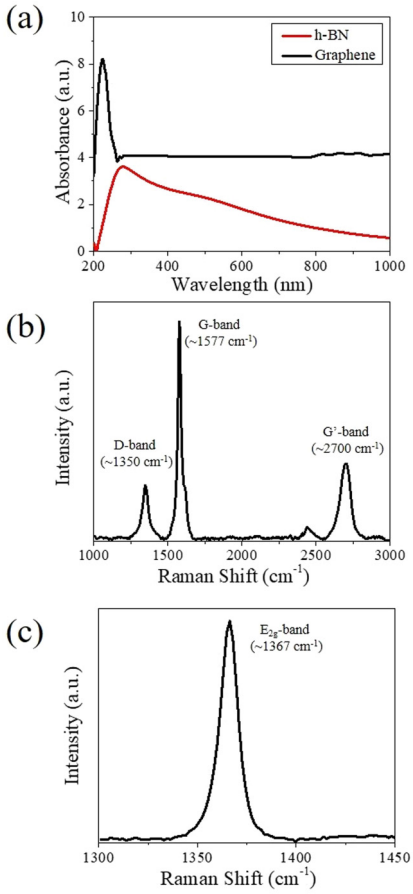


**FIG. 2.** (a) Optical absorption of graphene and h-BN as a function of wavelength. (b) Room temperature Raman spectra of the solution cast, annealed, and optimized graphene films. (c) Room temperature Raman spectra of the solution cast, annealed, and optimized h-BN films.

reveals its characteristic peak ($E_{2g}$ band) centered about a Raman wavenumber of 1367 $cm^{-1}$. In our prior studies,[42] we have computed the fragmentation rate of some typical 2D layered materials such as $MoS_2$, $WS_2$, and graphene when these were dispersed in solvents, where the fragmentation rate is a measure of the particle size reduction with ultrasonication time. From this work, we determined that the highest fragmentation rate generally occurred for sonication times ~30 min, and our h-BN material used here was sonicated well beyond these times. We infer the thickness of our printed structures based on our prior exploration, where the thickness of graphene changed from ~505 nm for 10 printing passes to ~1667 nm for 50 printing passes.[43]

Electrical characterization of the inkjet printed graphene-h-BN-graphene structure was conducted using the 450PM-B micromanipulator probe stage interfaced to an Agilent 4156A precision semiconductor parameter analyzer, along with the Lakeshore CRX-4K probe stage and Keysight B1500 semiconductor device analyzer, which was used for the capacitance (*C*)-frequency (*f*) measurements. Figures 3(a) and 3(b) depict the *I-V* characteristic data and the *C-f* response for the printed graphene-h-BN-graphene heterostructure, respectively. The h-BN layer in the capacitor shown in Fig. 1(b) was printed with a different number of passes, specifically ~6, 12, 20, 30, and 40 to compare the leakage current in the capacitor. In Fig. 3(a), the *I-V* shows high leakage currents for 6, 12, 20, and 30 passes of h-BN, although with an increasing number of passes, the current successively decreases. The top *I-V* characteristic in the inset for 40 passes for h-BN reveals leakage currents diminished to the nA range, suggesting that the optimized number of layers of 40 passes would be a good choice for further device studies. Figure 3(b) demonstrates the *C-f* measurement data for the printed capacitor (with 40 passes of h-BN) with various bias voltages applied at room temperature. At ~1 kHz, the maximum capacitance of ~62 pF was observed for each of the bias voltages, and with increasing frequency, the capacitance value decreases. When the frequency is low ~1 kHz, deeper traps participate particularly at the interfaces, and hence, the capacitance is high. As the frequency increases, the capacitor passes more charge across the plates in a given time resulting in a greater current flow

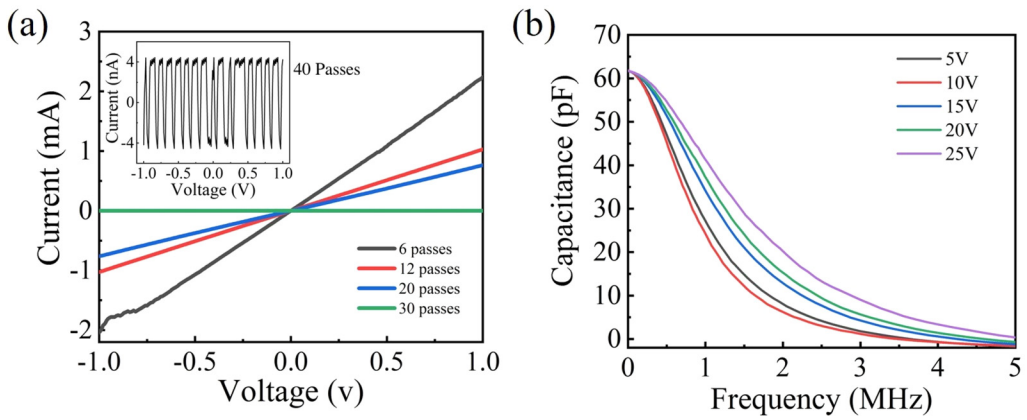


**FIG. 3.** (a) *I-V* characteristic of the inkjet printed graphene-h-BN-graphene capacitor, where h-BN was printed with 6, 12, 20, and 30 passes to explore the variation of the leakage current. With increasing passes, the leakage current decreased. The top inset shows that with 40 passes for the h-BN layer, the leakage current was reduced to the nA range. (b) The *C-f* response of the inkjet printed capacitor with 40 passes of h-BN, where the capacitance value was measured for various bias voltages at room temperature. At a low frequency of ~1 kHz, the maximum capacitance (~62 pF) was observed for each voltage, but with increasing frequency, the capacitance value decreased sharply.

through the capacitor, which decreases the capacitance. The same phenomena were observed for all bias voltages.

### B. Semiconducting $WS_2$ integrated with graphene for capacitors

Besides dielectric (h-BN) and conducting (graphene) inks, the dissolution of semiconducting 2D materials, specifically $WS_2$, was also investigated for ink formulation. The $WS_2$ powder was used at a concentration of 30 mg/ml for all our experiments. For horn tip sonication, $WS_2$ powder was taken in two separate glass beakers and 20 ml of the C/T/EC solution mixture was again added. This was the minimum amount of solution required for horn tip sonication. A minimum [HT (low)] and a maximum power amplitude [HT (high)] were used, and the total sonication time was 6 h. Sonication was performed at these conditions since these conditions did not lead to overheating the solutions, which potentially initiates degradative mechanisms and oxidation in the materials. The Fujifilm DMP-2800 series Dimatix Material Printer consisting of 16 inkjet nozzles was used to print graphene-$WS_2$-graphene heterostructure devices, and annealing for each layer was performed at 250 °C for 2 h to ensure much of the solvent desorbs from the printed film. A cartridge and a platen temperature of ~40 and 60 °C, respectively, were used during the printing.

Figure 4(a) shows the *I-V* characteristics of the exfoliated $WS_2$ through direct probing. The higher electrical conductivity of the HT (high) samples may be inferred to the lower resistance offered by the few-layer $WS_2$ nanosheets as the interlayer transport among van der Waals solids is usually found to be poor.[41] Figure 4(b) shows the room temperature Raman spectra of the exfoliated $WS_2$. In $WS_2$, two primary Raman active modes, the $A_{1g}$ mode arising from the out-of-plane vibrations related to the sulfur atoms occurs at ~418.8 $cm^{-1}$, while the *2LA(M)* mode occurs at ~352.4 $cm^{-1}$. The latter results from the in-plane displacement of tungsten and sulfur atoms, and both the $A_{1g}$ mode and the *2LA(M)* mode are shown in the spectra of Fig. 4(b).

Photoluminescence refers to the phenomenon of light emission from a material after an incoming photon is absorbed. The PL spectra intensity reaches a peak value when monolayers are produced suggesting direct interband transitions, and the intensity typically decreases and redshifts as the number of atomic layers increases. The PL spectra of the HT (high) sample in Fig. 4(c) showed a single, intense peak with a full-width-half-maximum ~142.6 nm and the shift in the wavelength (or equivalently energy) Δ for the PL peak was also noted for various samples. The Δ is blueshifted by ~147 nm from the weakly defined PL peak for the HT (low) sample as compared to the HT (high) sample. The higher PL intensity of HT (high) relative to HT (low) suggests a greater degree of exfoliation toward thinner molecular membranes. *C-V* measurements were conducted to analyze the nature of the graphene-$WS_2$ interface as shown by the data in Fig. 5. The probes were placed across two graphene contact pads by which the *C* was measured as a function of bias voltage *V* using the Keysight B1500A semiconductor device analyzer and the multifrequency CMU B1520A interfaced to it. When the frequency, *f*, applied is significantly low, a higher value of *C* is seen. This can be attributed to interfacial trapped states giving rise to additional capacitance.

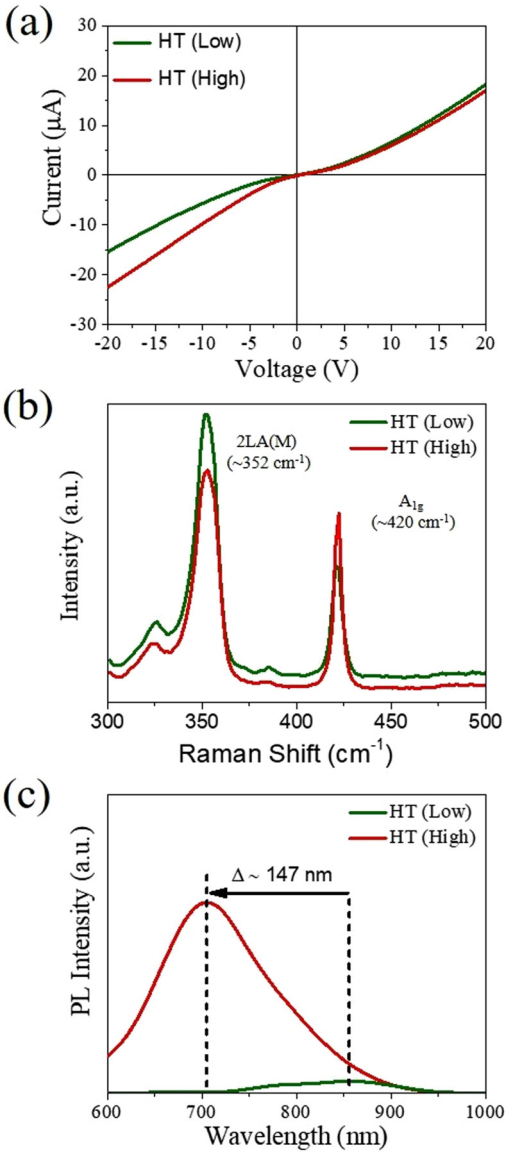


**FIG. 4.** (a) *I-V* characteristic for the HT (low) and HT (high) exfoliated $WS_2$ using direct probing. (b) Room temperature Raman spectra for the HT (low) and HT (high) exfoliated $WS_2$. (c) Photoluminescence characteristics of the HT (low) and HT (high) exfoliated $WS_2$ where a blueshift Δ ~ 147 nm is noted for the HT (high) sample, presumably due to the thinner membranes obtained at these conditions compared to HT (low).

The inverse proportionality of *C* values with increasing *f* is due to a decrease in the Schottky barrier height at the interface. No significant change in *C* values was observed when $f > 200$ kHz, which refers to the absence of a barrier against the flow of electrons. The highest *C* value was found at 20 kHz and at 0 V, where a value of ~324.88 pF was noted, while the lowest *C* ~2.81 pF was noted at

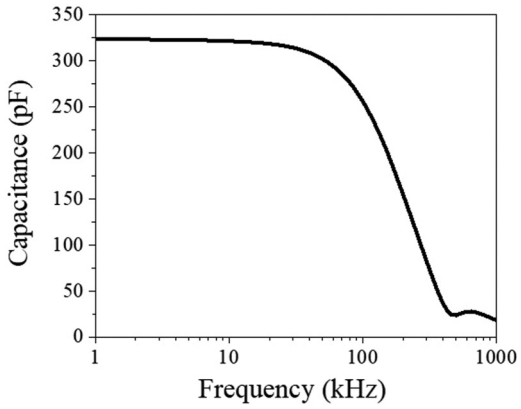


**FIG. 5.** Capacitance-voltage (*C-V*) measurements of the graphene-$WS_2$-graphene structures showing $C \sim 324$ pF at 1 kHz, which is more than 5× larger than the graphene-h-BN-graphene structures and is largely unchanged with frequency up to ~20 kHz.

the highest $f$ of ~3 MHz and at 0 V. The *C-V* measurements not only assist in the prediction of the formation of the depletion region but also in predicting the charging and discharging of the capacitance.[38,39] The inks and fabricated devices showed stability for over 3 months. These results are indicative of promising material performance for potential RF and microwave devices emerging from inkjet printing of 2D van der Waals solids.

## III. CONCLUSIONS

In conclusion, this work revealed that HT sonication resulted in promising dispersions of semiconducting $WS_2$, dielectric h-BN, and conducting graphene inks. From the *I-V* measurements, as the number of passes for printing the h-BN layer within graphene electrodes was increased, the leakage currents successively decreased. The *C-f* measurement data for the printed capacitor (with 40 passes of h-BN) with graphene electrodes showed that at ~1 kHz, the maximum capacitance of ~62 pF was observed, and with increasing frequency, the capacitance value decreases. The inkjet printed graphene-$WS_2$-graphene heterostructure devices were also constructed using HT sonication, where the *C-f* measurements revealed that $C$ as high as ~324.88 pF was observed, which was largely frequency independent up to ~20 kHz. This is in contrast with the h-BN layer integrated with graphene electrodes, where the measured $C$ was more than ~5 times lower over the range of frequencies tested and also exhibited a strong decay as frequency increased from 1 kHz.

## ACKNOWLEDGMENTS

We acknowledge the support received from the Army Research Office (Grant No. W911NF-15-1-0425) that enabled us to pursue this work. A.B.K. also acknowledges the support received from the PACCAR Technology Institute and Endowed Professorship.

## REFERENCES

[1]K. S. Novoselov, A. K. Geim, S. V. Morozov, D. A. Jiang, Y. Zhang, S. V. Dubonos, I. V. Grigorieva, and A. A. Firsov, Science **306**, 666 (2004).
[2]K. S. Novoselov, D. Jiang, F. Schedin, T. J. Booth, V. V. Khotkevich, S. V. Morozov, and A. K. Geim, Proc. Natl. Acad. Sci. U.S.A. **102**, 10451 (2005).
[3]A. B. Kaul, J. Mater. Res. **29**, 348 (2014).
[4]A. J. Chaves, R. M. Ribeiro, T. Frederico, and N. M. R. Peres, 2D Mater. **4**, 025086 (2017).
[5]J. H. Kim, J. H. Jeong, N. Kim, R. Joshi, and G.-H. Lee, J. Phys. D Appl. Phys. **52**, 083001 (2018).
[6]J. Kim, S. Byun, A. J. Smith, J. Yu, and J. Huang, J. Phys. Chem. Lett. **4**, 1227 (2013).
[7]K. F. Mak, C. Lee, J. Hone, J. Shan, and T. F. Heinz, Phys. Rev. Lett. **105**, 136805 (2010).
[8]W. Zhao, Z. Ghorannevis, L. Chu, M. Toh, C. Kloc, P.-H. Tan, and G. Eda, ACS Nano **7**, 791 (2012).
[9]Q. H. Wang, K. Kalantar-Zadeh, A. Kis, J. N. Coleman, and M. S. Strano, Nat. Nanotechnol. **7**, 699 (2012).
[10]M. Ye, D. Winslow, D. Zhang, R. Pandey, and Y. Yap, Photonics **2**, 288 (2015).
[11]M.-S. Alejandro, K. Hummer, and L. Wirtz, Surf. Sci. Rep. **70**, 554 (2015).
[12]D. Lembke, S. Bertolazzi, and A. Kis, Acc. Chem. Res. **48**, 100 (2015).
[13]E. Yalon *et al.*, Nano Lett. **17**, 3429 (2017).
[14]G. Eda, T. Fujita, H. Yamaguchi, D. Voiry, M. Chen, and M. Chhowalla, ACS Nano **6**, 7311 (2012).
[15]S. H. Lee, D. Lee, W. S. Hwang, E. Hwang, D. Jena, and W. J. Yoo, Appl. Phys. Lett. **104**, 193113 (2014).
[16]A. S. Pawbake, R. G. Waykar, D. J. Late, and S. R. Jadkar, ACS Appl. Mater. Interfaces **8**, 3359 (2016).
[17]N. Perea-López, A. L. Elías, A. Berkdemir, A. Castro-Beltran, H. R. Gutiérrez, S. Feng, and R. Lv, Adv. Funct. Mater. **23**, 5511 (2013).
[18]H.-S. Kim, M. Patel, J. Kim, and M. S. Jeong, ACS Appl. Mater. Interfaces **10**, 3964 (2018).
[19]D. Ovchinnikov, A. Allain, Y.-S. Huang, D. Dumcenco, and A. Kis, ACS Nano **8**, 8174 (2014).
[20]M. Buscema, J. O. Island, D. J. Groenendijk, S. I. Blanter, G. A. Steele, H. S. J. van der Zant, and A. Castellanos-Gomez, Chem. Soc. Rev. **44**, 3691 (2015).
[21]H. Chen, H. Liu, Z. Zhang, K. Hu, and X. Fang, Adv. Mater. **28**, 403 (2016).
[22]C. Li, C. Han, Y. Zhang, Z. Zang, M. Wang, X. Tang, and J. Du, Sol. Energy Mater. Sol. Cells **172**, 341 (2017).
[23]H. Guo, C. Lan, Z. Zhou, P. Sun, D. Wei, and C. Li, Nanoscale **9**, 6246 (2017).
[24]N. Petrone, T. Chari, I. Meric, L. Wang, K. L. Shephard, and J. Hone, ACS Nano **9**, 8953 (2015).
[25]A. S. Aji, P. Solís-Fernández, H. G. Ji, K. Fukuda, and H. Ago, Adv. Funct. Mater. **27**, 1703448 (2017).
[26]Y. Yu *et al.*, ACS Photonics **4**, 950 (2017).
[27]M. Hirano and S. Miyake, Appl. Phys. Lett. **47**, 683 (1985).
[28]C. Cong, J. Shang, X. Wu, B. Cao, N. Peimyoo, C. Qiu, L. Sun, and T. Yu, Adv. Opt. Mater. **2**, 131 (2014).
[29]Y. Niu *et al.*, Nanomaterials **8**, 725 (2018).
[30]J. A. Desai, N. Adhikari, and A. B. Kaul, MRS Adv. **2**, 3691 (2017).
[31]D. Fadil, R. F. Hossain, G. A. Saenz, and A. B. Kaul, J. Mater. Chem. C **5**, 5323 (2017).
[32]A. Delgado, J. A. Catalan, H. Yamaguchi, C. N. Villarrubia, A. D. Mohite, and A. B. Kaul, MRS Adv. **1**, 2303 (2016).
[33]V. Nicolosi, M. Chhowalla, M. G. Kanatzidis, M. S. Strano, and J. N. Coleman, Science **340**, 1226419 (2013).
[34]A. G. Kelly, D. Finn, A. Harvey, T. Hallam, and J. N. Coleman, Appl. Phys. Lett. **109**, 023107 (2016).
[35]H. Park, T. K. Kim, S. W. Cho, H. S. Jang, S. I. Lee, and S.-Y. Choi, Sci. Rep. **7**, 40091 (2017).

[36]S. Pang, H. N. Tsao, X. Feng, and K. Müllen, Adv. Mater. **21**, 3488 (2009).
[37]M. Michel, C. Biswas, and A. B. Kaul, Appl. Mater. Today **6**, 16 (2017).
[38]R. F. Hossain, I. G. Deaguero, T. Boland, and A. B. Kaul, NPJ 2D Mater. Appl. **1**, 28 (2017).
[39]N. Adhikari, A. Bandyopadhyay, and A. B. Kaul, MRS Adv. **2**, 3715 (2017).
[40]L. Peng, X. Peng, B. Liu, C. Wu, Y. Xie, and G. Yu, Nano Lett. **13**, 2151 (2013).
[41]J. A. Desai, N. Adhikari, and A. B. Kaul, RSC Adv. **9**, 25805 (2019).
[42]S. Mazumder, J. A. Catalan, A. Delgado, H. Yamaguchi, C. N. Villarrubia, A. D. Mohite, and A. B. Kaul, Compos. Sci. Technol. **192**, 107687 (2019).
[43]J. A. Desai, S. Chugh, M. Michel, and A. B. Kaul, J. Mater. Sci. Mater. Electron. **30**, 12500 (2019).